JOURNAL OF AIRCRAFT
Vol. 45, No. 5, September–October 2008

Investigation of Rotor Blade Structural Dynamics and Modeling Based on Measured Airloads

Jimmy C. Ho*
Georgia Institute of Technology, Atlanta, Georgia 30332
and
Hyeonsoo Yeo† and Robert A. Ormiston‡
Aeroflightdynamics Directorate (AMRDEC),
Ames Research Center, Moffett Field, California 94035

DOI: 10.2514/1.34025

The work presented herein treats measured airloads from the UH-60A Airloads Program as prescribed external loads to calculate the resulting structural loads and motions of a rotor blade. Without the need to perform any aerodynamic computations, the coupled aeroelastic response problem is reduced to one involving only structural dynamics. The results, computed by RCAS and CAMRAD II, are compared against measured results and against each other for three representative test points. The results from the two codes mostly validate each other. Seven more test points, with responses computed by RCAS, to form thrust and airspeed sweeps are evaluated to better understand key issues. One such issue is an inability to consistently predict pushrod loads and torsion moments well, and this is found to be amplified at the two test points with the highest thrust coefficient. For these two test points, harmonic analysis reveals that the issue is due to excessive amounts of 5/rev response that stem from high levels of 5/rev pitching moment excitation. Another issue that concerns all test points is that the phase of the 1/rev blade flapping motion is not predicted well, which reflects the high sensitivity of this quantity that is developed due to having a first flap frequency of approximately 1/rev. Results also show that current force-velocity relationships, used in describing the lead–lag damper, are not satisfactory to consistently yield accurate inboard chordwise bending moment predictions. Overall, the investigation here, conducted with numerous test points, further confirms the methodology of prescribing measured airloads for assessing the structural dynamics capability of a computational tool.

Nomenclature

C_W	=	weight coefficient
F_D	=	lead–lag damper force
M_{tip}	=	hover tip Mach number
M_∞	=	freestream Mach number
R	=	blade radius
V_D	=	lead–lag damper velocity
r	=	radial coordinate
σ	=	solidity
μ	=	advance ratio

Introduction

THE complicated nature of rotor blade aerodynamics and its interdependence on structural dynamics are major hindrances to accurately predicting blade loads by computational tools. It is difficult to identify whether sources of inaccuracies originate from deficiencies in aerodynamic or structural dynamic predictions. To assess the structural dynamic aspect, researchers specify measured airloads from experiment as prescribed external loads and then compare the resulting response with the measured response. Sweers [1] applied this approach to data collected from flight tests of the XH-51A. Wind-tunnel tests and flight tests provided the data for Esculier and Bousman [2] to use this approach with the CH-34 rotor blade. Torok and Goodman [3] also prescribed measured airloads from wind-tunnel tests of a scaled UH-60A rotor for this purpose.

The current investigation, as well as most others of this nature from recent years, focuses on predicting the structural response of a UH-60A rotor blade from prescribing airloads, as measured from the NASA/Army UH-60A Airloads Program [4]. Data from this program include airloads and structural loads at several radial locations along the blade span, and so it is especially useful for the purpose here. Ormiston [5] examined the blade structural dynamic response from measured airloads for a high-speed case using the comprehensive rotorcraft analysis code RCAS [6]. In that work, the calculation of the rotor blade structural dynamic response when airloads are prescribed is referred to as "mechanical airloads." Another previous study [7] showed results using UMARC for the same high-speed case as well as a low-speed case and one with high thrust.

A set of criteria should be satisfied for one to obtain good correlation between calculations and measurements using this approach. The criteria are accurate measurements of airloads, accurate measurements of structural loads, accurate rotor blade properties, a correct modeling of the problem, and an analysis tool that properly solves the governing equations. Errors in any one of these criteria compromise the correlation.

Results of previous works, from prescribing measured airloads, generally show good correlation between calculations and measurements; however, certain issues and uncertainties do exist. Although flatwise and chordwise bending moments are reasonably well predicted, torsion moment (TM) and pushrod load (PL) predictions are less accurate. In addition, phase angle predictions of the 1/rev blade flapping response are consistently poor. Previous works include calculations from several different codes, but these results are rarely based on the same modeling assumptions and inputs so as to justify a direct comparison of the results. The scope of

Received 13 August 2007; revision received 27 March 2008; accepted for publication 10 April 2008.

*Graduate Research Assistant, Guggenheim School of Aerospace Engineering, 270 Ferst Drive; JHo@gatech.edu. Member AIAA.
†Research Scientist, U.S. Army Research, Development, and Engineering Command, Mail Stop 215-1.
‡Chief Scientist, Aeromechanics, U.S. Army Research, Development, and Engineering Command, Mail Stop 215-1. Fellow AIAA.

previous investigations is also typically limited to no more than a few test cases.

The objectives of the present work are thus to expand the scope of this investigation by analyzing many more test cases and also to carefully compare results from two advanced rotorcraft codes for a representative subset of the chosen cases. The UH-60A Airloads Program covered a large range of flight test points, and so the work here examines more of its test points to help address the previously identified issues and uncertainties. One aspect of the present strategy is to examine groups of test points for which a single primary flight-test parameter is varied, for example, the weight coefficient or advance ratio, to help identify trends or dependencies that may be related to the particular parameter. The two advanced rotorcraft codes mentioned are RCAS and CAMRAD II [8].

The general presentation of results is now described. Three test points, which represent a wide range of aerodynamic environments, are first analyzed to identify the broad issues. These issues are next examined in more detail by observing the results from test points that vary only in the weight coefficient and then for test points that vary only in the advance ratio. The "thrust sweep," referred to here as the analysis of test points that vary in C_W, isolates the effects of blade stall progression. The "speed sweep," referred to here as the analysis of test points that vary in μ, isolates forward speed progression effects such as compressibility and retreating blade stall. Establishing the validity of a code is greatly enhanced by the comparison of results from two codes together along with the test data. For this reason, RCAS and CAMRAD II are used for the representative test points whereas only RCAS is used for the in-depth examination of the speed and thrust sweeps. Lastly, results from different modeling of the lead–lag damper are presented. Note that two sets of results, each with a different value for the pushrod stiffness, are provided for all test points investigated in this paper due to the uncertainty [9] of this parameter.

UH-60A Airloads Program

An objective of the UH-60A Airloads Program was to acquire data pertinent to rotor blade aeromechanics. For this purpose, the blades of the UH-60A used for testing were highly instrumented with pressure transducers, strain gauges, and accelerometers. The aircraft performed a wide variety of flight conditions including hover, level flight, maneuvers, climbs, and descents to collect data. The steady level flight conditions, in terms of μ and C_W/σ, chosen for the current investigation are listed in Table 1.

The specific flight counters, which have already been alluded to, will now be properly identified. The three chosen representative test points for this work are flight counters 8534, 8513, and 9017. As shown by Potsdam et al. [10], counter 8534 is a high-speed case featuring prominent compressibility effects on the advancing side, counter 8513 is a low-speed case with blade-vortex interactions, and counter 9017 is a high-thrust case featuring dynamic stall. The high-speed case examined by Ormiston [5] is flight counter 8534. The study [7] conducted using UMARC examined counter 8534 as its high-speed case, counter 8515 as its low-speed case, and counter 9017 as its high-thrust case.

Radial locations at which airloads and structural loads of the blade were measured are now described. Absolute pressures were measured at $r/R = 0.225$, 0.40, 0.55, 0.675, 0.775, 0.865, 0.92, 0.965, and 0.99. The airload data have a 1.5 deg azimuthal resolution. Flatwise bending moments (FBMs) were measured at $r/R = 0.113$, 0.2, 0.3, 0.4, 0.5, 0.6, 0.7, 0.8, and 0.9. Chordwise bending moments (CBMs) were measured at $r/R = 0.113$, 0.2, 0.3, 0.4, 0.5, 0.6, 0.7, and 0.8. Torsion moments were measured at $r/R = 0.3$, 0.5, 0.7, and 0.9. The structural load data have a 7.5 deg azimuthal resolution.

Table 1 UH-60A flight-test counters

Counter	C_W/σ	μ
8515	0.078	0.110
8513	0.079	0.153
8525	0.078	0.232
8528	0.079	0.308
8534	0.078	0.368
8422	0.089	0.242
8817	0.101	0.223
8914	0.111	0.232
9020	0.120	0.245
9017	0.133	0.237

Modeling and Analysis

The comprehensive rotorcraft analysis codes RCAS and CAMRAD II are used for modeling and analysis. Structural modeling of the blade is developed from a common UH-60A master input database, which was developed by Yeo and has been used extensively for recent studies of UH-60A [5,11,12]. The swash plate is not modeled and not included. Any couplings with the drive train and fuselage are ignored. It is also assumed that no coupling, as with dissimilar blades or swash plate flexibility, exists between the blades; thus, a single-bladed model is sufficient. Figure 1 reveals the modeling details of the rotor hub with blade hinges, pitch control, and the lead–lag damper. The blade is composed of 13 nonlinear beam elements. A series of rigid bars and spring elements are used to represent the pitch control linkage. The motion of the pitch control slide element, which is located at the base of the pushrod, is specified with the collective and 1/rev cyclic controls. The pitch controls are chosen for individual counters to match the measured pitch bearing rotation waveform, thus treating blade pitch as an input. Three coincident hinge elements are offset from the center of rotation. The three hinge elements allow for simultaneous flap, lag, and pitch rotations of the blade. With the exception of the nonlinear beam element, all structural elements are geometrically exact with no small angle or small deformation assumptions.

Measured airloads and damper loads (an exception to this is in evaluating different modeling of the lead–lag damper) are applied as external loads to an isolated single-bladed rotor. Measured normal force, chord force, and pitching moment are prescribed along the blade span. Measured airload data are available at nine radial locations, and so interpolated airloads, by cell averaging, are prescribed at 26 radial locations for RCAS and at 21 radial locations for CAMRAD II analysis. The azimuthal resolution of the prescribed loads is every 1.5 deg for RCAS and every 5 deg for CAMRAD II. RCAS and CAMRAD II both used harmonic balance to calculate structural response. All results shown are obtained using ten harmonics, because including more does not result in any significant changes.

Blade Frequency Results

It is paramount to accurately determine the dynamic characteristics for an understanding of the response of any dynamics system. Figures 2 and 3 show the rotor blade frequency calculations as a

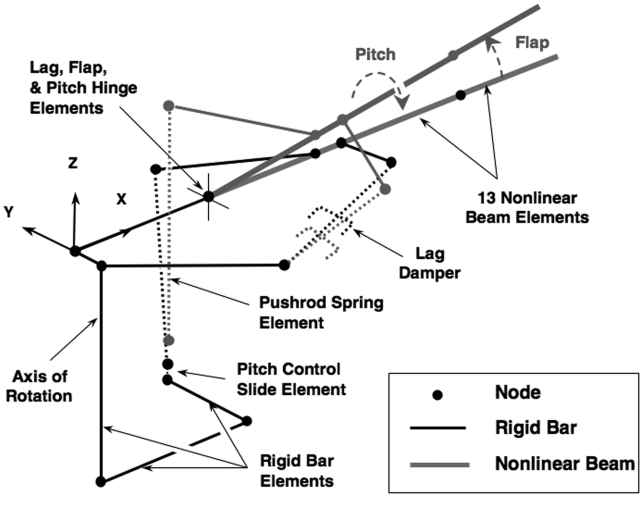

Fig. 1 Finite element model showing hub details.

function of the rotor speed for pushrod stiffness values of 364 and 1090 ft · lb/ deg, respectively. The soft value was inferred indirectly by Shanley [13], under a NASA contract, by comparing analysis and test data. On the other hand, the stiff value was determined experimentally from direct measurements of the aircraft hardware by Kufeld and Johnson [9]. The results from previous publications were performed using either one of the two values. The frequencies shown are for a nominal zero collective pitch (defined at the three-quarter blade radius) with damping set to zero. The frequency predictions by the two codes differ by less than a percent in most cases and serve as validation to some extent. A thick vertical line has been drawn to indicate the nominal rotor speed. The labeling of the modes corresponds to the nominal rotor speed, because participation by each of the contrasting motions depends on the rotor speed for coupled modes. Pushrod stiffness does not alter the frequencies of the three lowest modes. Above the first three modes, strong couplings exist among the modes so that pushrod stiffness does become a factor. Although the fourth mode is predominantly a torsion mode, the next two modes are so highly coupled that their labeling is merely a judgment call.

Note that the model includes pushrod damping, which increases the modal damping of the torsion mode. Pushrod damping effects give about 1% modal damping to the first torsion mode when using the stiff pushrod, but the compliance of the soft pushrod increases modal damping of this mode to about 10%. This may account for differences between the two pushrods in subsequent results.

RCAS and CAMRAD II Comparisons

Counter 8534, High Speed

Flight counter 8534 represents the test point with the highest advance ratio ($\mu = 0.368$) from the UH-60A Airloads Program. With a hover tip Mach number of $M_{\text{tip}} = 0.642$ and a freestream Mach number of $M_\infty = 0.236$, the blade operated in transonic flow. It was shown [10] that advancing blade negative lift was evident outboard.

The pitch bearing rotation waveform is shown in Figs. 4 and 5 for the soft and stiff pushrods, respectively. The good agreement with the measured data is representative of all counters, because the control inputs of the calculated results were iterated to match the blade measured pitch motion. Note that the total range of oscillatory blade pitch angle for this counter is approximately 24 deg, which is large enough that linear analyses based on approximate small angle kinematic assumptions are not appropriate.

The oscillatory flatwise bending, chordwise bending, and torsion moments and pushrod load waveforms are shown in Figs. 6 and 7 for the soft and stiff pushrods, respectively. The word "oscillatory" is used here in reference to periodic waveforms with the mean removed. Calculated and measured flatwise bending moments are in good agreement, except that the measured values lag the calculations by 7–10 deg in azimuth. The calculations and measurements agree well for the chordwise bending moments except that the peak amplitude at and just inboard of the midspan, occurring near 180 deg azimuth, is not well predicted, which was suggested [5] to be due to neglecting the coupling between the rotor and engine. The behaviors of torsion moments and pushrod load, which are interdependent, are predicted reasonably well in the first and second quadrants, but are not well predicted on the retreating side.

As would be expected for calculations with the same modeling, the two codes show little deviation from each other. With the exception of subtle differences, RCAS and CAMRAD II are in virtual agreement for the flatwise and chordwise bending moments. RCAS and CAMRAD II predictions of pushrod load and torsion moment waveform share the same characteristics but differ slightly in amplitudes at certain azimuths.

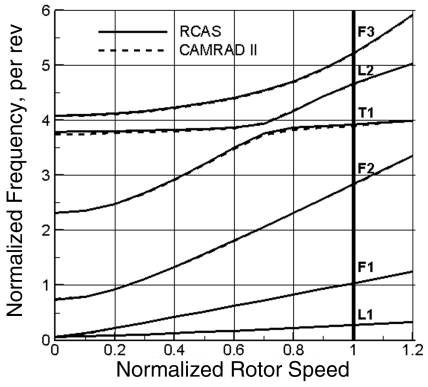

Fig. 2 Rotor blade frequencies vs rotor speed for zero collective pitch with a pushrod stiffness of 364 ft · lb/ deg.

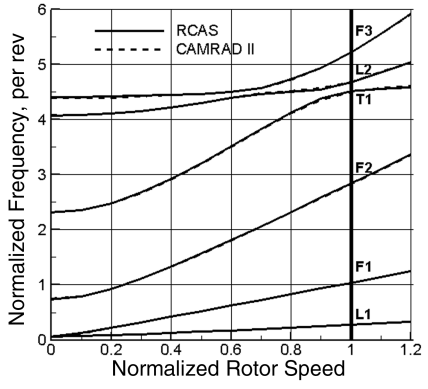

Fig. 3 Rotor blade frequencies vs rotor speed for zero collective pitch with a pushrod stiffness of 1090 ft · lb/ deg.

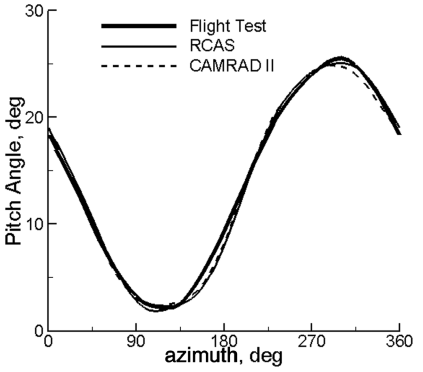

Fig. 4 Blade root pitch control angle for counter 8534 ($C_W/\sigma = 0.078$, $\mu = 0.368$) with calculations using a pushrod stiffness of 364 ft · lb/ deg.

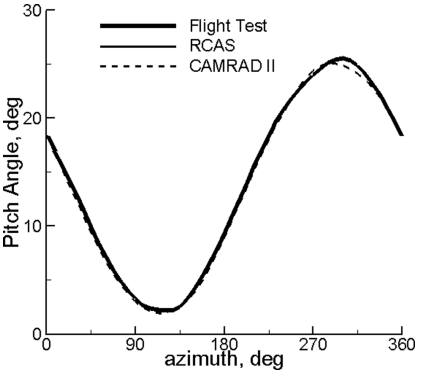

Fig. 5 Blade root pitch control angle for counter 8534 ($C_W/\sigma = 0.078$, $\mu = 0.368$) with calculations using a pushrod stiffness of 1090 ft · lb/ deg.

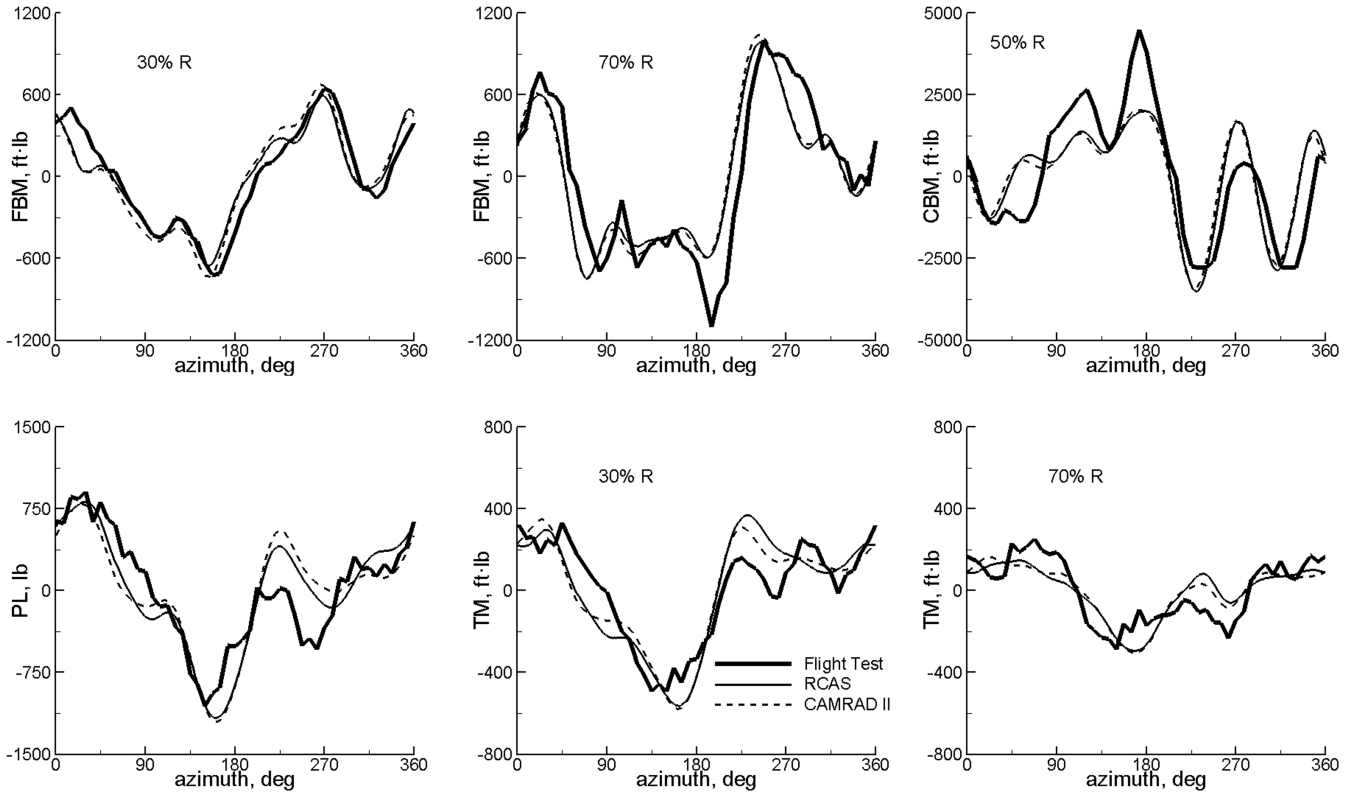

Fig. 6 Oscillatory waveforms of structural loads for counter 8534 ($C_W/\sigma = 0.078$, $\mu = 0.368$) with calculations using a pushrod stiffness of 364 ft · lb/ deg.

Not surprising, a comparison of Figs. 6 and 7 reveal that pushrod stiffness alters the characteristics of the pushrod loads and torsion moments, whereas it has little effect on flatwise and chordwise bending moments. Its effects are most easily seen on the retreating side.

Counter 8513, Low Speed

The airloads from the low-speed ($\mu = 0.153$) case that is flight counter 8513 are significantly impacted by the presence of blade-vortex interactions, which are visible from the calculated visualization of the wakes [10].

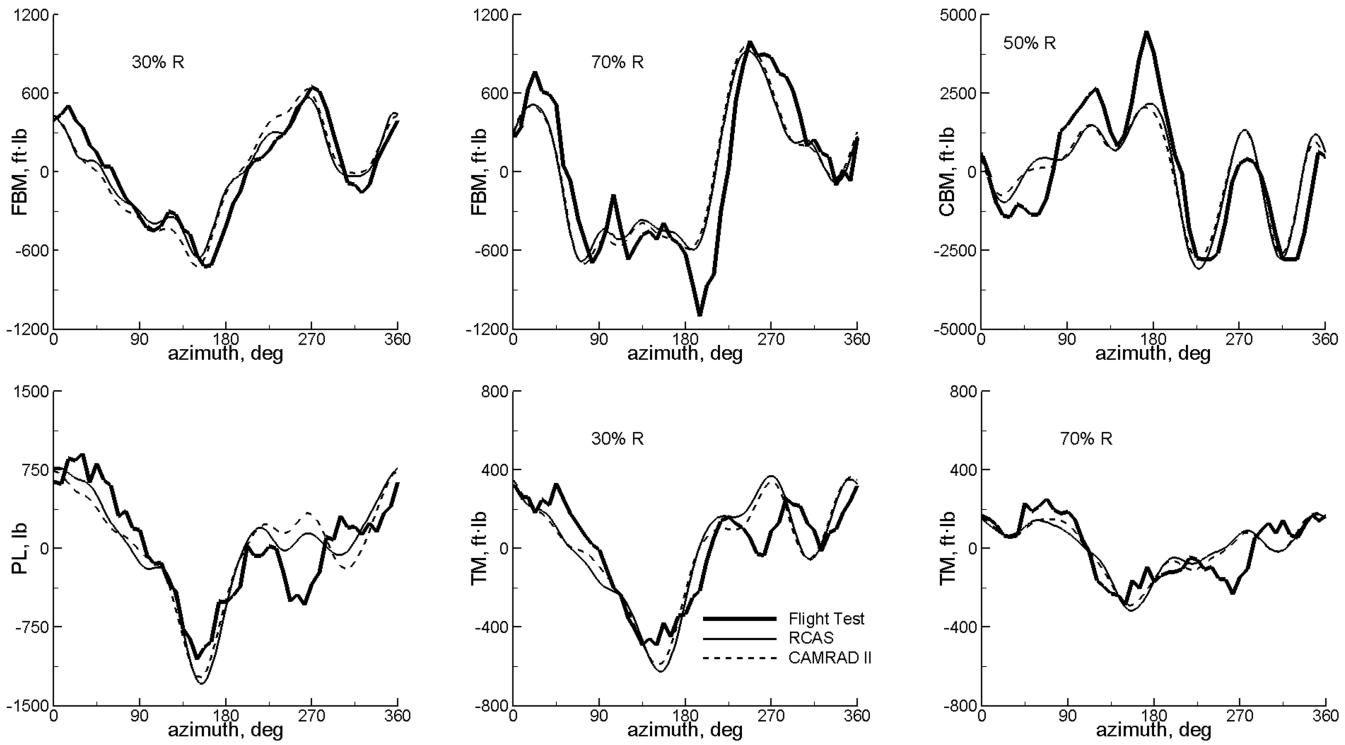

Fig. 7 Oscillatory waveforms of structural loads for counter 8534 ($C_W/\sigma = 0.078$, $\mu = 0.368$) with calculations using a pushrod stiffness of 1090 ft · lb/ deg.

The oscillatory waveforms of several loading parameters are shown in Figs. 8 and 9 for the soft and stiff pushrods, respectively. As with counter 8534, the predicted flatwise bending moments correlate well with the measurements, while still exhibiting a slight lead in azimuth. The chordwise bending moment predictions are in good agreement and, unlike counter 8534, the deficiency of a lower predicted peak amplitude is much less severe. Neglecting the spikes in the test data and some deviations in the fourth quadrant the , torsion moments are generally well predicted. RCAS and CAMRAD II still show excellent agreement with one another in both flatwise and chordwise bending moments, but some differences do appear in the fourth quadrant for torsion moments. Pushrod stiffness again had only minor effects on flatwise and chordwise bending moments, whereas it still showed some effects on torsion moments.

Counter 9017, High Thrust

Flight counter 9017 flew at an intermediate speed ($\mu = 0.237$) and at the highest value of C_W/σ (0.133, a result of flying at 17,000 ft) of any level flight test points from the testing program. The blade operated in the transonic regime with a hover tip Mach number of $M_{\text{tip}} = 0.665$ and a freestream Mach number of $M_\infty = 0.157$. Aerodynamic predictions for this case would be challenging as the unsteady environment also included dynamic stall and wake interactions.

The predicted values of oscillatory flatwise and chordwise bending moments, as shown in Figs. 10 and 11 for the soft and stiff pushrods, respectively, show good agreement with test data. The chordwise bending moment is presented at $11.3\%R$, because measured data are unavailable at other radial locations due to malfunctions in the strain gauges. Predicted flatwise bending moments lead measured values by small amounts in azimuth as before.

A major finding, as seen in Figs. 10 and 11, is that the correlation of pushrod load and torsion moments between predictions and measurements is now worse for this high C_W case compared with the two previous counters. The primary cause is that the predicted fifth harmonic, especially with the stiff pushrod, is far greater than the measured value. This disparity between the results from the two pushrods might be related to their difference in modal damping of the first torsion mode, which is approximately 10% for the soft pushrod and 1% for the stiff pushrod. A discussion on the excessive amount of fifth harmonic content is given in the discussion on thrust sweep results in a later section of the paper.

RCAS and CAMRAD II results show mostly the same behavior. CAMRAD II results exhibit a slightly higher level of the fifth harmonic in pushrod loads and torsion moments as well as slightly higher amplitudes in its bending moments.

Note that UMARC results, from a previous study [7] and mentioned in [14], appear to yield better correlation. It is now understood that the UMARC results presented contain additional damping; thus, it does not display the issue of excessive magnitudes in the fifth harmonic in pushrod load and torsion moments.

Detailed Investigations Conducted by Incorporating More Test Points

Issues which arose in the initial survey of representative test points are now examined in greater detail by observing additional results from test points that vary in only one key flight parameter. Results from a thrust sweep are shown by choosing flight counters that vary in their value of C_W while having approximately the same flight speed. Results are next shown from a speed sweep, which features counters that vary in μ while having approximately the same weight coefficient. From the three representative test points, significant issues are encountered in predicting pushrod loads and torsion moments. Another issue, which was not mentioned in showing the results of the representative test points but which was identified previously [5], is the poor prediction in the phase angle of the 1/rev

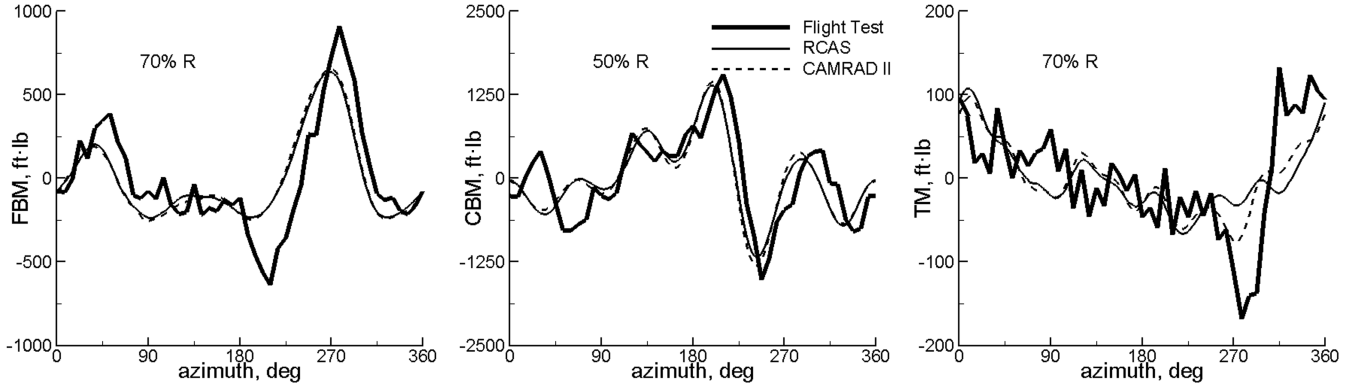

Fig. 8 Oscillatory waveforms of structural loads for counter 8513 ($C_W/\sigma = 0.079$, $\mu = 0.153$) with calculations using a pushrod stiffness of 364 ft · lb/deg.

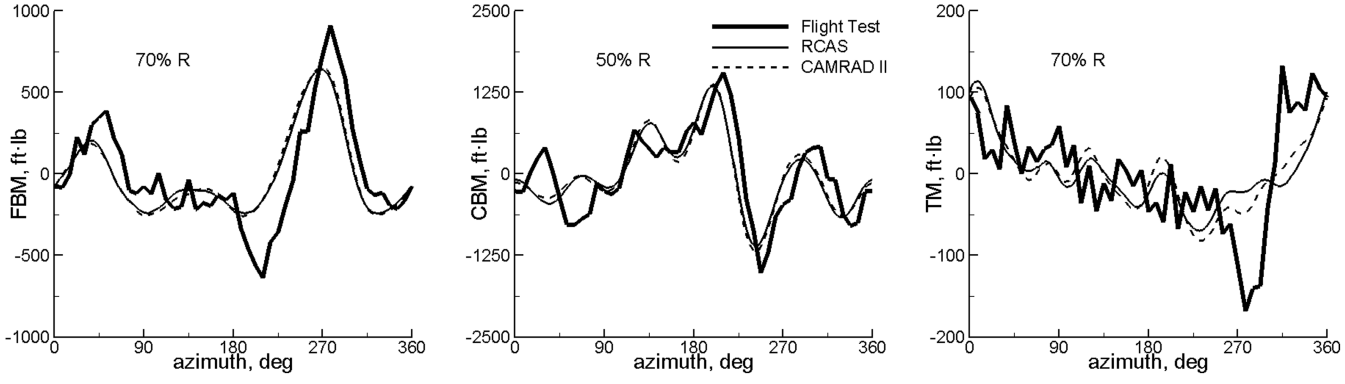

Fig. 9 Oscillatory waveforms of structural loads for counter 8513 ($C_W/\sigma = 0.079$, $\mu = 0.153$) with calculations using a pushrod stiffness of 1090 ft · lb/deg.

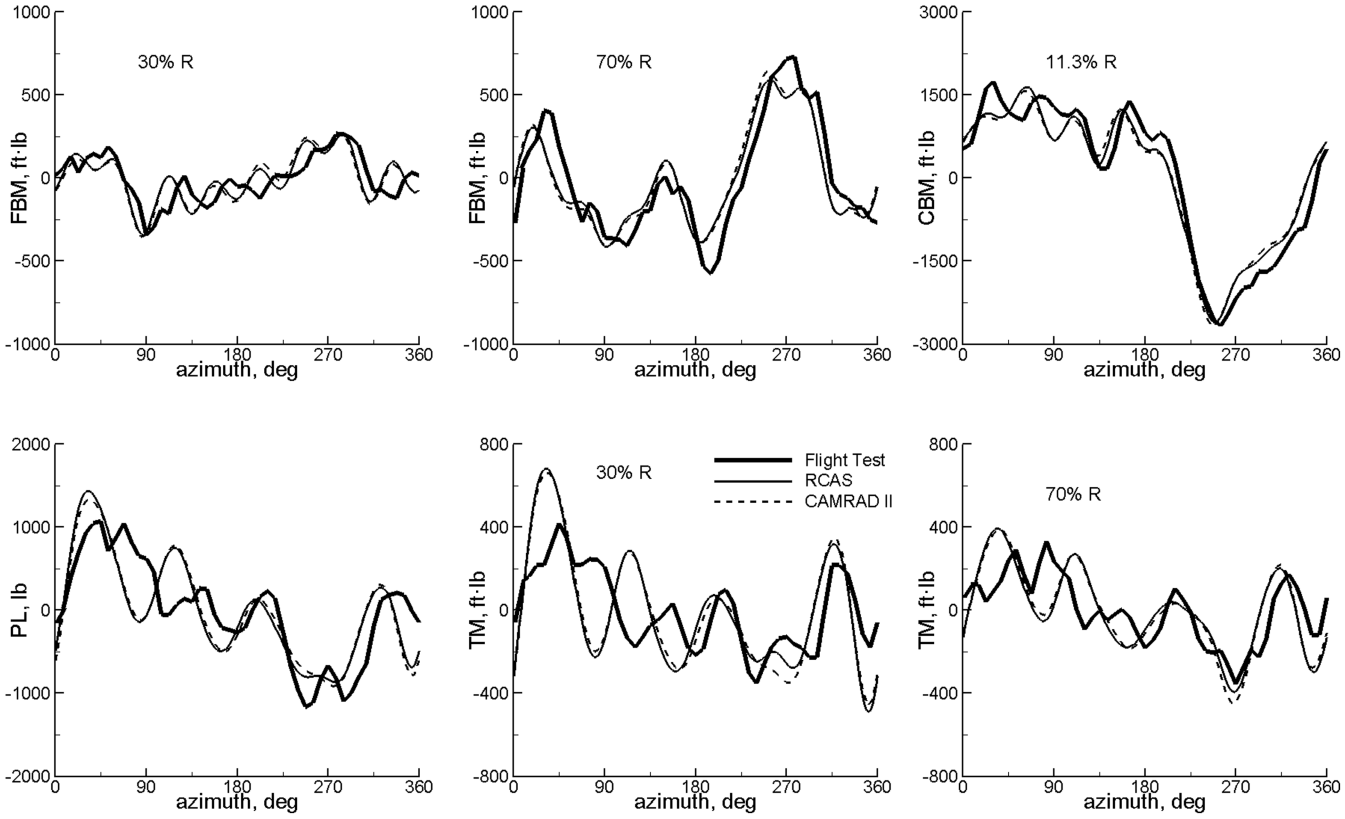

Fig. 10 Oscillatory waveforms of structural loads for counter 9017 ($C_W/\sigma = 0.133$, $\mu = 0.237$) with calculations using a pushrod stiffness of 364 ft · lb/ deg.

blade flapping response. The sections that follow will consist of one forming the sweep in C_W, one the sweep in μ, one that specifically addresses the 1/rev flapping response, and one that discusses different modeling of the lead–lag damper load.

Computed results presented from this point forward are solely from RCAS. The mostly close agreement between RCAS and CAMRAD II, as shown, makes it unlikely that CAMRAD II would yield significant differences.

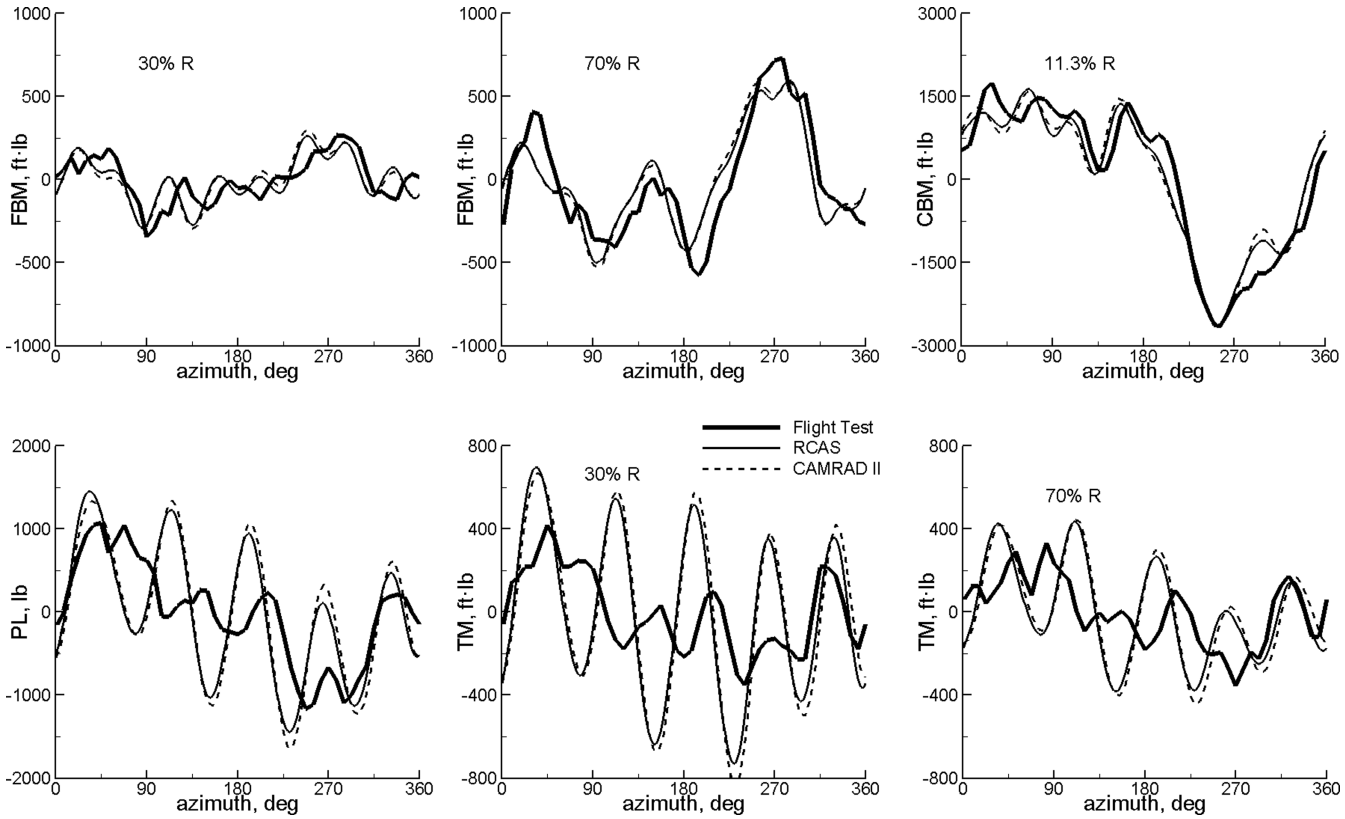

Fig. 11 Oscillatory waveforms of structural loads for counter 9017 ($C_W/\sigma = 0.133$, $\mu = 0.237$) with calculations using a pushrod stiffness of 1090 ft · lb/ deg.

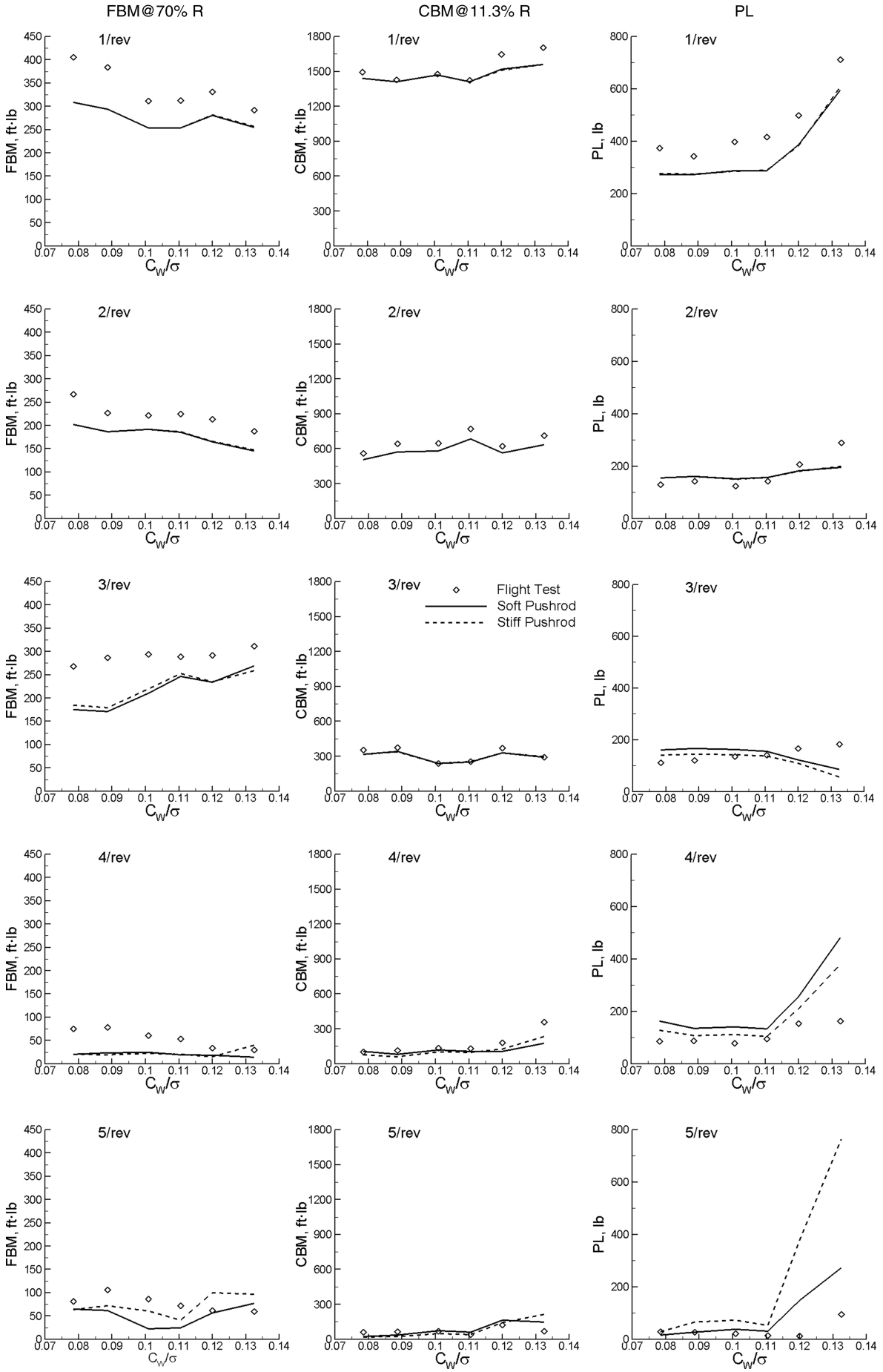

Fig. 12 First five harmonic magnitudes of FBM at 70%R, CBM at 11.3%R, and PL for counters investigated in thrust sweep, using a pushrod stiffness of 364 and 1090 ft · lb/ deg at an advance ratio of $\mu \cong 0.235$.

Thrust Sweep

Results from varying C_W are especially of interest due to the poor pushrod load and torsion moment predictions from the high C_W case of flight counter 9017. The strategy here is to display the harmonics of loading parameters, as these are easily compared, between calculations and measurements as functions of C_W. This also facilitates the identification of the response behavior in relation to the excitation harmonics as well as to the system natural frequencies.

Six counters, each with an advance ratio of $\mu \cong 0.235$, are selected for the thrust sweep. The six counters are counter 8525, 8422, 8817, 8914, 9020, and 9017. As reflected in Table 1, the value of C_W/σ here ranged from 0.078 to 0.133. The flight altitude was adjusted to fly at the desired value of C_W/σ. Counter 9017, which has already been examined, represents the case with the highest value of C_W/σ.

The first five harmonics of flatwise and chordwise bending moments at chosen locations are shown in Fig. 12. Chordwise bending moment data are shown at $11.3\%R$, because the measured data are unavailable in the cases of counters 9020 and 9017 at other radial locations due to malfunctions in the strain gauges. Predicted flatwise bending moment harmonics correlate well with measured harmonics for the most part. The first three harmonics of flatwise bending moment at $70\%R$ are predicted to be less than the experimental value, although the general trends are captured as C_W is varied. The vast majority of chordwise bending moment at the root is due to its nearby damper load, which is prescribed from the measured results. For this reason, RCAS has excellent agreement for chordwise bending moment at the root, except for the first harmonic at the two highest thrust levels.

Figure 12 also shows the first five harmonics of pushrod load. The predicted magnitudes of the 4/rev contents are excessive for these two high-thrust cases, yet they are overshadowed by the 5/rev predictions. These unacceptably high 5/rev predictions also create a difference between using the soft and stiff pushrods, whereas differences between the two are negligible to moderate elsewhere. The stiff pushrod produced dramatically greater levels than the already too high numbers from the soft pushrod, which is consistent with what was discussed for counter 9017. The results here imply the onset of blade stall for the higher C_W cases.

The cause of the high 5/rev response, in pushrod load and torsion moments, will now be sought by examining the excitation harmonics from the airloads. This shortcoming in prediction is unique to the two counters featuring the highest levels of C_W. The issue is more apparent for $C_W/\sigma = 0.133$, and it might seem that prediction capabilities degrade with an increase of C_W if C_W is sufficiently high. Figure 13 shows the magnitude of the measured pitching moment harmonics at all nine radial locations from the thrust sweep. It reveals that the fifth harmonic experiences a sudden rise in prominence, in relation to the other harmonics, when the thrust level reaches $C_W/\sigma = 0.120$ and prevails more at $C_W/\sigma = 0.133$. Note that the 5/rev pitching moment spike starts at $r/R = 0.865$, which is also where the pitching moment stall spikes appear in the airload waveform. Results from Potsdam et al. [10] show a clear double stall spike in the fourth quadrant that is consistent with the 5/rev frequency. Contributions by the first harmonic overwhelm all others, and so its values are omitted to visualize the others more clearly. It was verified that higher harmonics not shown are of less influence.

The high 5/rev predicted pushrod loads and torsion moments are caused by high 5/rev pitching moment excitations, but the question now shifts to why high 5/rev responses are not not evident in the flight test data. One possibility is that operating at higher levels of C_W at increased collective pitch would shift the blade frequencies and mode shapes so that the responses become more sensitive to 5/rev excitations. However, calculations for higher pitch angles showed that the blade frequencies are virtually constant with respect to the collective in the range of collectives used for our analysis. Unfortunately, there does not appear to be an obvious explanation for this problem. It is likely that small errors in the modeling and blade properties influence the coupled torsion frequency, mode shape, and response characteristics near 5/rev and that these effects become prominent for a large 5/rev pitching moment excitation. It is noted that the 5/rev pushrod load is not well predicted even before stall

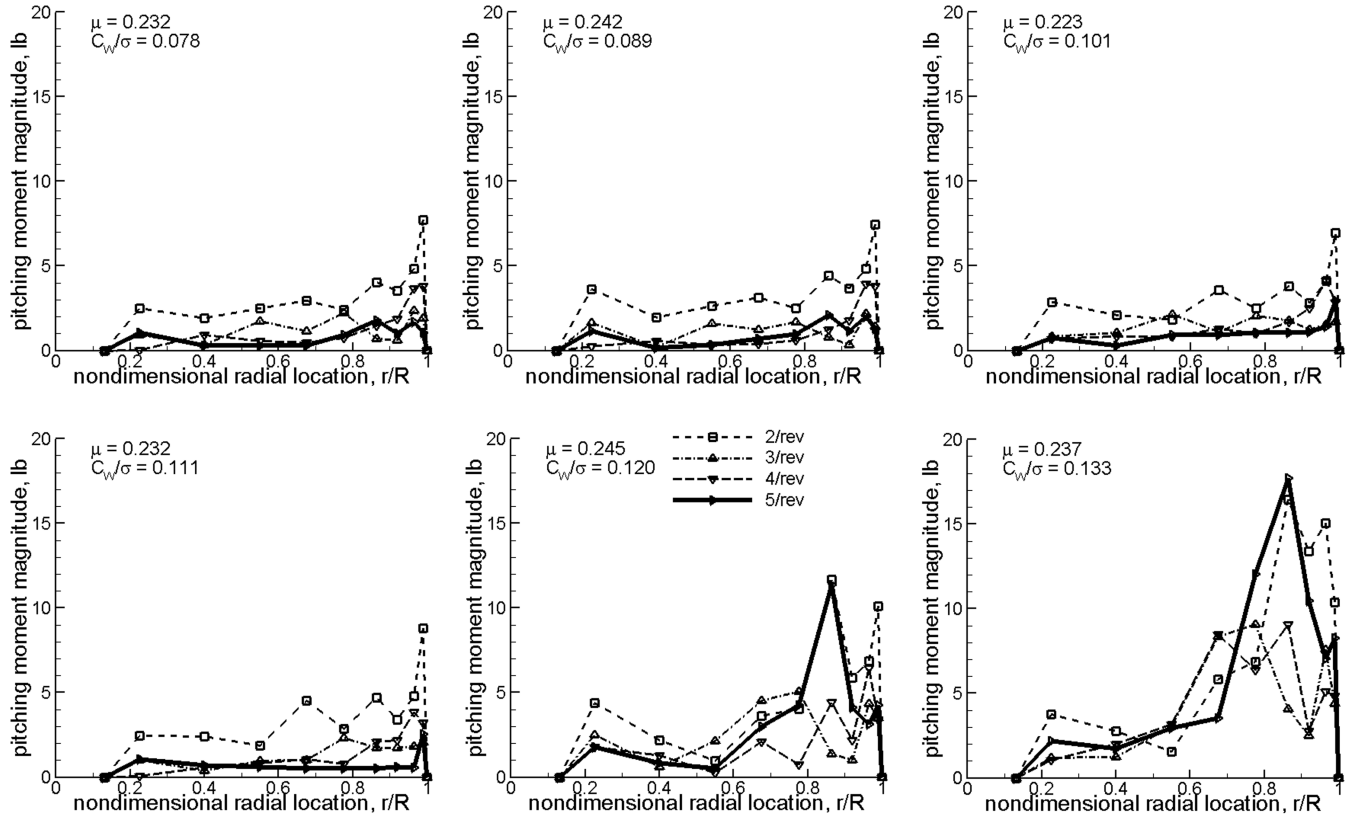

Fig. 13 Flight-test pitching moment magnitudes of second to fifth harmonics for counters investigated in thrust sweep at an advance ratio of $\mu \cong 0.235$.

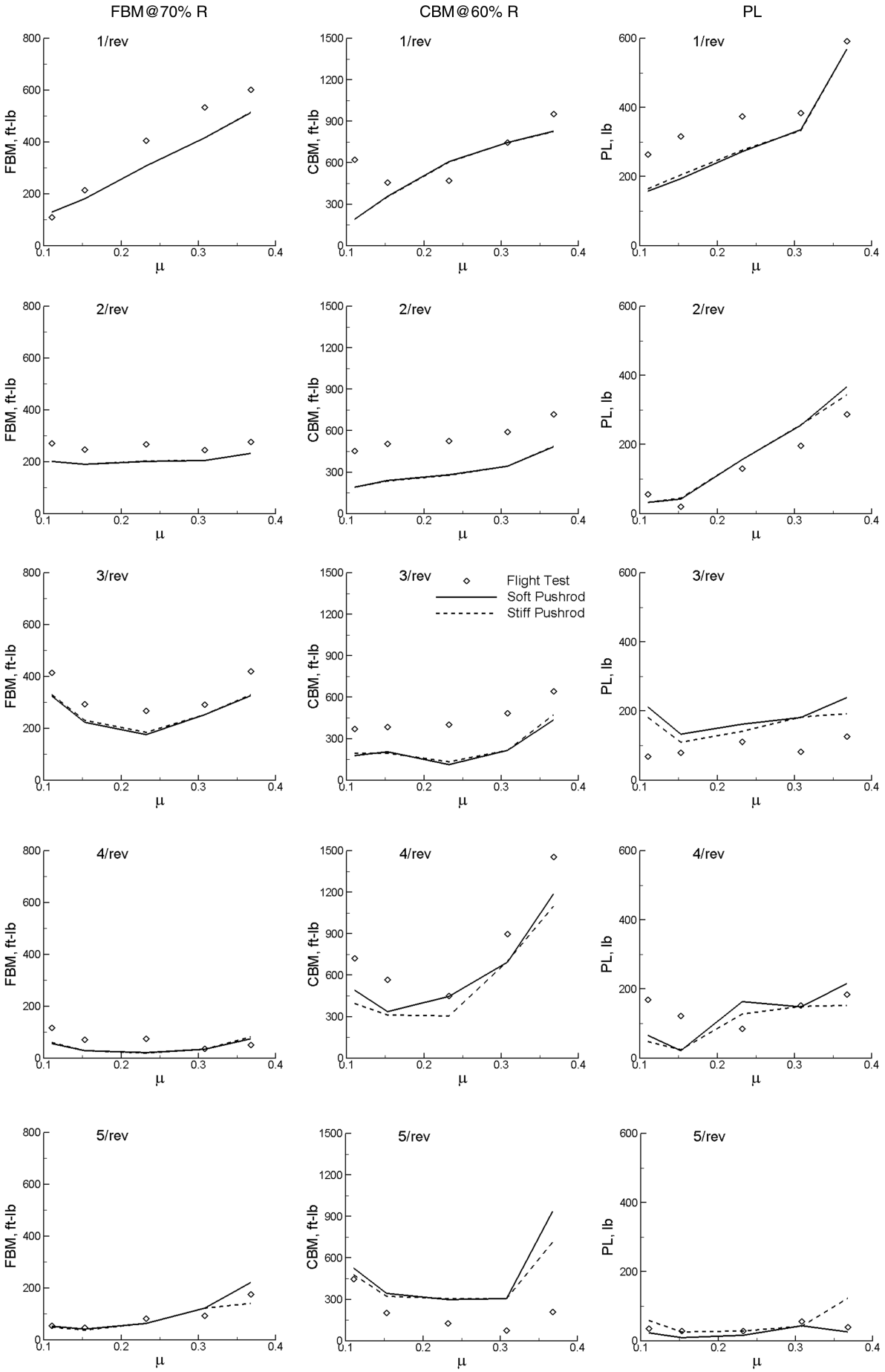

Fig. 14 First five harmonic magnitudes of FBM at 70%R, CBM at 60%R, and PL for counters investigated in speed sweep, using a pushrod stiffness of 364 and 1090 ft · lb/deg at a thrust of $C_W/\sigma \cong 0.079$.

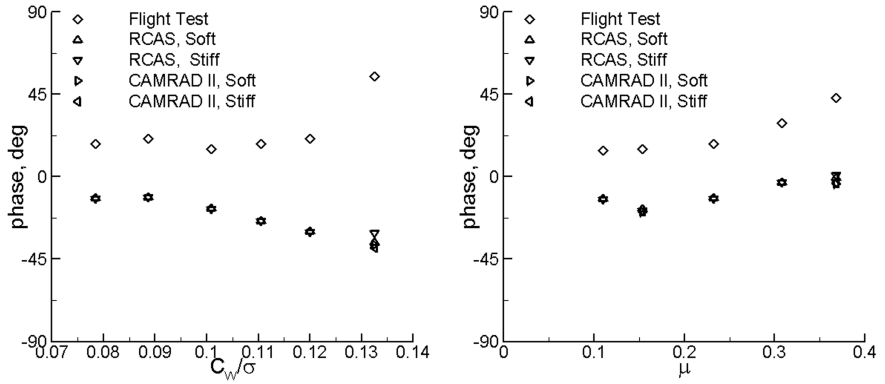

Fig. 15 First harmonic phase of blade flapping motion about the flap hinge for counters investigated: a) thrust sweep, and b) speed sweep.

begins, but its magnitude is negligible at low C_W levels. When stall occurs and the pitching moment excitation greatly increases, the 5/rev pushrod load becomes large and the error becomes very apparent. Therefore, for the present problem, the presumed modeling and blade property errors are only significant when stall occurs.

Speed Sweep

The strategy here is to again display the harmonics of loading parameters between the calculations and measurements, but now as functions of advance ratio. Correlations of pushrod loads and torsion moments are of primary interest due to problems in predicting them well.

Five counters, each with a thrust level of $C_W/\sigma \cong 0.079$, are selected for the speed sweep. The counters are 8515, 8513, 8525, 8528, and 8534. The value of m ranged from 0.110 to 0.368 for this sweep, as given in Table 1. Counter 8534, which has already been examined individually, represents the case with the highest value of μ. Counter 8513 has also received individual attention, whereas counter 8525 ($C_W/\sigma = 0.078$, $\mu = 0.232$) represents the lowest thrust case from the thrust sweep.

In general, airloads, and hence structural loads, increased as airspeed was increased. This observation is visible in Fig. 14, which shows the first five harmonics of pushrod load and bending moments at chosen locations. As with the thrust sweep, RCAS predicts a lower magnitude for each of the first three harmonics of flatwise bending moment at 70%R despite capturing the correct trend as speed is varied. Although not shown here, this lower prediction in magnitude of the three lowest harmonics appeared at 60 and 50%R as well. The chordwise bending moment at 60%R is predicted well due to prescribing the measured damper load.

One trend, which surfaced in the thrust sweep as well, is in regard to the flatwise bending moments. From counters 8534, 8513, and 9017, predictions from both RCAS and CAMRAD II exhibit a small lead in azimuth over the measured data. This phase difference is present in all counters forming both the thrust and speed sweeps.

Blade Flapping Motion

For all ten cases examined, a noticeable discrepancy exists in the first harmonic content of the blade motion about its flap hinge between the RCAS predictions and measured results. For $\mu = 0.368$, it was demonstrated by Ormiston [5] that nearly all the discrepancy is due to an unexplained 46-deg phase shift of the 1/rev component. It has been shown [14] for all ten counters examined here that it is again the 1/rev component that is responsible for most of the discrepancy in oscillatory motion. In investigating the CH-34 rotor, Esculier and Bousman [2] also noted poor correlations with the 1/rev component.

The phase angles of the first harmonics in blade flapping, from both the thrust and speed sweeps, are shown in Fig. 15. CAMRAD II predictions from the three representative test points are included in Fig. 15 and are in agreement with RCAS predictions. The phase difference between predictions and measurements is most severe for the case of the highest μ and the highest C_W/σ in the speed and thrust sweeps, respectively. Ormiston [5] discussed this in detail and attributed the difference to the sensitivity in flapping response, which developed from having a first flap frequency of approximately 1/rev. Results from Fig. 15 show this is a consistent systematic difference and the specific source is as yet undiscovered. It is noteworthy that the phase difference is nearly constant for the speed sweep except for the case of the highest μ. For the thrust sweep, the phase difference is also nearly constant for the cases of $C_W/\sigma = 0.078$, 0.089, and 0.101. For the cases in which $C_W/\sigma \geq 0.111$, the phase difference increases with increasing values of C_W/σ. As rotor blade stall begins for the two cases of the highest C_W/σ, the phase difference increases significantly in a similar fashion to the 5/rev responses of its pushrod load and torsion moments.

Lead–Lag Damper Modeling

The results presented thus far have all been generated by prescribing the measured damper load, and so this section will focus on results from computing the damper load by assuming its force-velocity relationships. A nonlinear model, as specified by Howlett [15], and a linear model are two analytical models that are currently in use to model the force-velocity relationships. The nonlinear model specifies F_D as a constant value of 4000 lb if $V_D \geq 0.583$ ft/s and -4000 lb if $V_D \leq -0.583$ ft/s. It has a nonlinear behavior within the interval $|V_D| < 0.583$ ft/s, which is shown in Fig. 16. The linear model, also shown in Fig. 16, has a constant slope of 4405 lb/(ft/s) for all velocities.

The damper load strongly influences the root chordwise bending moment, and so the results shown will focus on this quantity from applying the soft pushrod. Figure 17 shows the correlation of this quantity with the flight test for the three representative test points from applying the nonlinear model and the linear model, and also from prescribing the measured damper load. The predicted

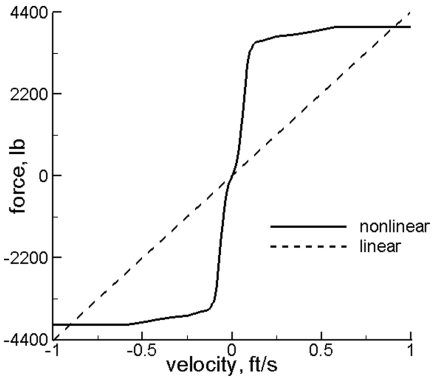

Fig. 16 Force-velocity curves for the lead–lag damper.

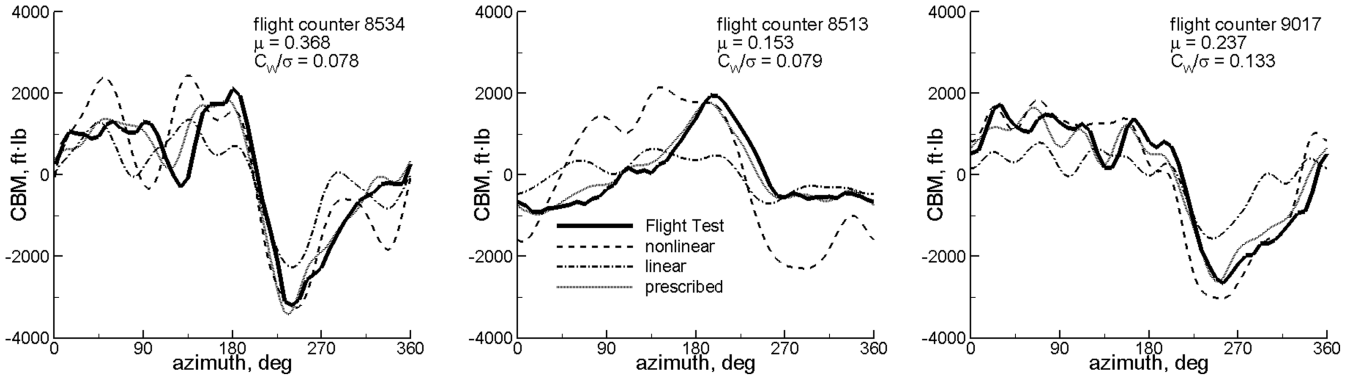

Fig. 17 Oscillatory CBM waveform at the root for three representative flight counters using a pushrod stiffness of 364 ft · lb/deg with the nonlinear damper model, the linear damper model, and prescribing the measured damper load.

waveforms naturally correlate well with the flight test if prescribing the measured damper load for all three flight counters. Correlations from applying the linear model are poor for all three flight counters and thus indicate that this linear model is not adequate. Correlations from applying the nonlinear model may be considered adequate for flight counters 8534 and 9017, but not for counter 8513. Results, not shown here, from altering the force-velocity relationships of the nonlinear model on its nonlinear interval indicate that counter 8513 is more sensitive than the other two counters in this regard. It would seem that experiments are required to obtain accurate force-velocity relationships. Bauchau and Liu [16] recently applied a physics-based damper model along with prescribing measured airloads to counter 8534 and still found deficiencies.

Conclusions

The blade structural response from different test points of the UH-60A Airloads Program was predicted from two rotorcraft comprehensive codes, RCAS and CAMRAD II, by applying measured airloads as prescribed external loads. The analysis was conducted for an isolated single-bladed rotor with controls set to match the measured blade pitch. A total of ten test points were analyzed, encompassing a thrust sweep and a speed sweep in level flight conditions. The calculated structural loads and blade motions were then compared with the measured results to draw the following conclusions:

1) The investigation of additional cases confirmed the general success of previous studies, which used a limited number of flight test points. In general, the issues previously identified remain unresolved, although these issues are now much more clearly defined. This focus should help further investigations to better understand the issues.

2) The close agreement in predictions between RCAS and CAMRAD II provides significant confidence that each of these codes accurately reflects the very similar modeling and analysis assumptions they are based on. Generally good agreement with measured blade loads confirms that the structural dynamics modeling, analysis, blade properties, and experimental measurements are generally accurate. Limited differences between the calculations and test data are likely due to errors in modeling, blade properties, or the experimental measurements. The small differences noted for torsion moments, pushrod loads, and the blade 1/rev flapping phase warrant additional investigation.

3) It is observed, for all test points, that calculated flatwise bending moments lead the measured values by a small amount in azimuth.

4) Among the structural loading parameters compared, pushrod loads and torsion moments showed the most difference between the calculations and test data. Of the test points analyzed, these differences became most significant for the two highest thrust coefficient cases. In those two cases, the predicted response exhibits an excessive amount of 5/rev content, and it is due to high levels of 5/rev pitching moment excitation that the modeling and property data inaccuracies are much more prominent.

5) Additional results revealed that the previously identified phase error of 1/rev blade flapping response is present for a wide range of speed and thrust conditions. The difference is relatively independent of the flight condition and suggests a specific source rather than a random measurement error. The flapping response is highly sensitive due to the close proximity of the first flap frequency to 1/rev. This difference also existed for a previous study on the CH-34 rotor blade.

6) Force-velocity relationships, used in calculating the load of the lead–lag damper, are not accurate enough to consistently attain good correlations for inboard chordwise bending moments. If good correlations are desired without prescribing the measured damper load, then experiments may be needed to better characterize the force-velocity relationships.

References

[1] Sweers, J. E., "Theoretical Prediction of Airloads and Structural Loads and Correlation with Flight Test Measurement," United States Army Aviation Materiel Laboratories TR-68-22C, May 1968.

[2] Esculier, J., and Bousman, W. G., "Calculated and Measured Blade Structural Response on a Full-Scale Rotor," *Journal of the American Helicopter Society*, Vol. 33, No. 1, Jan. 1988, pp. 3–16.

[3] Torok, M. S., and Goodman, R. K., "Analysis of Rotor Blade Dynamics Using Model Scale UH-60A Airloads," *Journal of the American Helicopter Society*, Vol. 39, No. 1, Jan. 1994, pp. 63–69.

[4] Kufeld, R. M., Balough, D. L., Cross, J. L., Studebaker, K. F., Jennison, C. D., and Bousman, W. G., "Flight Testing of the UH60-A Airloads Aircraft," *Proceedings of the 50th Annual Forum of the American Helicopter Society*, American Helicopter Society, Alexandria, VA, May 1994, pp. 557–578.

[5] Ormiston, R. A., "An Investigation of the Mechanical Airloads Problem for Evaluating Rotor Blade Structural Dynamics Analysis," *Proceedings of the American Helicopter Society 4th Decennial Aeromechanics Specialist Meeting*, American Helicopter Society, Alexandria, VA, Jan. 2004.

[6] Saberi, H., Khoshlahjeh, M., Ormiston, R. A., and Rutkowski, M. J., "Overview of RCAS and Applications to Advanced Rotorcraft Problems," *Proceedings of the American Helicopter Society 4th Decennial Aeromechanics Specialist Meeting*, American Helicopter Society, Alexandria, VA, Jan. 2004.

[7] Sitaraman, J., Datta, A., Baeder, J., and Chopra, I., "Coupled CFD/CSD Prediction of Rotor Aerodynamic and Structural Dynamic Loads for Three Critical Flight Conditions," *Proceedings of the 31st European Rotorcraft Forum*, Paper 77, Sept. 2005.

[8] Johnson, W., "Technology Drivers in the Development of CAMRAD II," *Proceedings of the American Helicopter Society Aeromechanics Specialist Meeting*, American Helicopter Society, Alexandria, VA, Jan. 1994, pp. PS3.1–PS3.14.

[9] Kufeld, R. M., and Johnson, W., "The Effect of Control System Stiffness Models on the Dynamic Stall Behavior of a Helicopter," *Journal of the American Helicopter Society*, Vol. 45, No. 4, Oct. 2000, pp. 263–269.

[10] Potsdam, M., Yeo, H., and Johnson, W., "Rotor Airloads Prediction Using Loose Aerodynamic/Structural Coupling," *Journal of Aircraft*, Vol. 43, No. 3, May–June 2006, pp. 732–742. doi:10.2514/1.14006

[11] Yeo, H., Bousman, W. G., and Johnson, W., "Performance Analysis of a Utility Helicopter with Standard and Advanced Rotors," *Journal of the American Helicopter Society*, Vol. 49, No. 3, July 2004, pp. 250–270.

[12] Datta, A., and Chopra, I., "Validation and Understanding of UH-60A Vibratory Loads in Steady Level Flight," *Journal of the American Helicopter Society*, Vol. 49, No. 3, July 2004, pp. 271–287.

[13] Shanley, J. P., "Validation of UH-60A CAMRAD/JA Input Model," Sikorsky Aircraft SER-701716, Stratford, CT, Nov. 1991.

[14] Ho, J. C., Yeo, H., and Ormiston, R. A., "Investigation of Rotor Blade Structural Dynamics and Modeling Based on Measured Airloads," *Proceedings of the 63rd Annual Forum of the American Helicopter Society*, American Helicopter Society, Alexandria, VA, May 2007, pp. 1720–1742.

[15] Howlett, J. J., "UH-60A Black Hawk Engineering Simulation Program: Volume 1—Mathematical Model," NASA CR-166309, Dec. 1981.

[16] Bauchau, O. A., and Liu, H., "On the Modeling of Hydraulic Components in Rotorcraft Systems," *Journal of the American Helicopter Society*, Vol. 51, No. 2, April 2006, pp. 175–184.